JOURNAL OF MATERIALS SCIENCE 21 (1986) 2356–2364

Inelastic deformation of (Ti, V)C alloys

Part 2 *Load relaxation studies*

VIVEK M. SURA*, D. L. KOHLSTEDT
Department of Materials Science and Engineering, Cornell University, Ithaca, New York 14853, USA

The high temperature plastic deformation of (Ti, V)C alloys was studied by load relaxation experiments. The deformation experiments were performed at 1200 to 1600° C on fully dense, single phase, polycrystalline TiC, TiC–25% VC, TiC–50% VC and TiC–75% VC, prepared by hot-pressing. The analysis of $\log\sigma$–$\log\dot{\varepsilon}$ data along with the evaluation of strain rate sensitivity ~ 0.9 to 1.5 and the grain size dependence ~ 2.6 indicates that the high temperature plastic deformation of these carbides occurs by grain-boundary diffusion, which is in accordance with hot-pressing results. Also, transmission electron microscopy of deformed samples, revealing little evidence for dislocation activity, supported this conclusion. The diffusion coefficients obtained in this study are in good agreement with those obtained for boundary diffusion, with the activation energy $\sim 390\,kJ\,mol^{-1}$ for TiC and $\sim 307 \pm 13\,kJ\,mol^{-1}$ for other compositions. A sharp decrease in the strength of (Ti, V)C alloys with the addition of VC is associated with the softening and/or melting of second phase material accumulated along the grain boundaries.

1. Introduction

A limited amount of work has been performed on the alloys of titanium–vanadium carbide. Hollox *et al.* [1] determined the room temperature hardness and the high temperature yield strength of single crystals of TiC–VC alloys having a carbon to metal ratio close to 0.85. They found that the room temperature hardness increases in a linear fashion from 19.7 ± 1.0 GPa for VC to 26.5 ± 0.5 GPa for TiC; in contrast, the high temperature critical resolved yield strength exhibits a maximum between TiC–80 % VC and TiC–60% VC. The critical resolved shear stress of TiC–67% VC is 420 MPa at 1400° C, while those of pure VC and pure TiC are ~30 and 50 MPa, respectively, at the same temperature. The temperature dependence of the critical resolved shear stress also differs from one alloy composition to the next. Hannink and Murray [2] studied the effect of cooling rate on the room temperature hardness of polycrystalline TiC–26% VC and TiC–78% VC with a carbon to metal ratio of 0.84. They observed that the hardness of the TiC-rich alloy is higher than that of the VC-rich alloy; both alloys have higher hardness than the parent carbides.

In this context, the present work was undertaken to study the plastic deformation of well characterized, fully dense, single phase, polycrystalline (Ti, V)C alloys prepared by hot-pressing. Load relaxation experiments were used to examine the high temperature mechanical properties. Microstructural analyses of undeformed and deformed samples were carried out to correlate these properties with structural variables. In addition, the temperature dependence, the strain rate sensitivity and the grain size dependence were evaluated to determine the rate-controlling mechanism operating during deformation.

2. Experimental details

2.1. Materials and sample preparation

Powders of four different compositions TiC, TiC–25 wt % VC, TiC–50 wt % VC and TiC–75 wt % VC were thoroughly dry mixed for a minimum of 6 h. The starting particle size distribution and purity of the TiC and VC powders which were used to fabricate samples are described in the companion paper [3]. The respective powder charges were placed in cylindrically shaped graphite dies of 6.35 mm inner diameter and 25.4 mm length. These powder batches were cold pressed at a pressure of 70 MPa, and then uniaxially hot-pressed at 1750° C, at 120 MPa for 60 min in an argon atmosphere. Throughout the heating period, a stress of 25 to 30 MPa was applied. Five to ten samples of each composition were hot-pressed.

To study the effect of grain size on the deformation behaviour, some samples of TiC–75% VC were annealed at 1900 and 2000° C for one hour in an argon atmosphere to permit grain growth. During annealing, samples were not surrounded by graphite powder.

Both the as-hot-pressed and the hot-pressed and annealed samples were cut and polished to prepare specimens 6.35 mm in diameter and 12 mm in length for load relaxation tests.

2.2. Experimental apparatus

The load relaxation tests were conducted in argon in the high temperature furnace described in the previous paper [3].

* *Present address*: IBM East Fishkill, Hopewell Junction, New York 12533, USA.

0022–2461/86 $03.00 + .12

A 455 kg load cell, with an output of 1 mV per 22.7 kg and a sensitivity of $\pm 1\,\mu$V, was used to determine the stress on the sample. The output from the load cell was measured with a digital voltmeter at the rate determined by a clock-interface. The clock-interface could be set to change its rate either manually or automatically, according to the needs of the test. The data were continuously recorded on a magnetic tape for subsequent computer analysis.

A stable temperature is essential in order to minimize thermal expansion effects in the testing machine and load train sufficiently to obtain data at strain rates below $10^{-6}\,\text{sec}^{-1}$. Accordingly, the deformation rig was housed in a 10 cm thick, fibreglass insulated box. The box was located in a well insulated room in which the temperature was controlled by a constant flow of cool air, modulated by a thermostat controlled heater. This arrangement provided temperature stability of better than $\pm 0.1^\circ$C in the vicinity of the furnace chamber. The testing machine was turned on only for a short time required to load the specimens, so as to minimize the heat generated from the motors.

Special precautions were taken to reduce the relaxation of the machine and load train. The two condensers in the damping network of the machine were shortened out, the preload springs on the top of the drive screws were tightened, and the grease between the crosshead and the drive screws was removed. All the connections in the load train were tightened under load. Less than 5% of the total load drop during the relaxation run can be attributed to thermal fluctuations and machine relaxation.

2.3. Experimental procedure

Constant-temperature load-relaxation tests were performed in the temperature range 1200 to 1600° C, by loading a given sample at a constant compression rate ($0.001\,\text{cm min}^{-1}$) to a predetermined load and then stopping the crosshead. During the loading stage, elastic energy is stored in the loading train; during the load relaxation stage, this energy is slowly transferred to the sample which underwent continuous inelastic deformation. Several load relaxation tests were performed on each sample at successively higher loads.

The load as a function of time was recorded throughout the loading and the relaxation periods. The rate of data collection was changed several times during the course of a run. The data of the loading part were collected at a rate of one reading per second to calculate accurately the elastic constant of the specimen plus machine. The relaxation of the load is very fast at the very beginning of the relaxation stage and continuously slows down. Consequently, for the first 2 min, ten data points sec^{-1} were recorded; for the next 15 to 20 min, one data point sec^{-1} was recorded; for the remainder of the run ($\sim$8 h to 6 d), the data were collected at a rate of one reading every 20 to 40 sec.

2.4. Data processing

The load–time data were analysed to obtain stress, σ, as a function of strain, ε, and strain rate, $\dot{\varepsilon}$. The plastic length of the sample can be calculated for both the loading region and the relaxation region using the following equation:

$$L(t) = L_0 - \dot{X}t + P(t)/K \quad (1)$$

where L_0 is the initial length, $\dot{X}$ the crosshead velocity, $P(t)$ the load at time t and K the combined elastic constant of the machine and the specimen. Note that in the relaxation region, $\dot{X} = 0$ hence

$$L(t) = L_1 + P(t)/K \quad (2)$$

where

$$L_1 = L_0 - X_t \quad (3)$$

and X_t is the total crosshead displacement, which can be calculated using $\dot{X}$ and the total loading time. Thus, knowing the plastic length at any time, σ and ε were calculated using the following relations:

$$\sigma(t) = P(t)\,L(t)/A_0 L_0 \quad (4)$$

$$\varepsilon(t) = -\ln L(t)/L_0 \quad (5)$$

where A_0 is the initial cross-sectional area. The strain rate during relaxation was calculated as

$$\dot{\varepsilon}(t) = \dot{L}(t)/L(t) = \dot{P}(t)/K/L(t) \quad (6)$$

The elastic constant K was calculated by measuring the slope of the load–time data from the loading part of the load relaxation test. The details of computing $\dot{P}(t)$ have been described previously [4, 5].

2.5. Microstructural observations

Specimens for optical microscopy as well as for scanning electron microscopy (SEM) were diamond cut from the hot-pressed samples and then polished by normal metallographic techniques. An etchant of 1 : 1 : 3 solutions of nitric, hydrofluoric, and lactic acids was used to reveal the microstructure. Grain size was determined by using a linear intercept technique with a correction factor of 1.5. Density of a sample at the end of a hot-pressing run was measured by the water immersion method.

X-ray diffraction was used to determine the major crystalline phases present and to calculate the lattice parameter of the as-hot-pressed samples. Portions of mechanically thinned samples were ion thinned to produce specimens for transmission electron microscopy (TEM). These foils were examined on a Siemens 102 transmission electron microscope and a JEOL 200CX scanning transmission electron microscope.

3. Results

3.1. Characterization of hot-pressed samples

The bulk compositions of these samples, as measured by an energy dispersive spectrometer on an SEM, were in excellent agreement with the desired composition. X-ray diffraction data demonstrated that all the samples were single phase, with the rock-salt structure. The lattice parameter, a, for each of the four compositions, as tabulated in Table I, agrees well with data in the literature [6].

Optical micrographs of the as-hot-pressed and the hot-pressed and annealed samples are shown in Figs 1 and 2, respectively. The as-hot-pressed samples are all $\sim > 99\%$ dense and have uniform grain sizes. In

TABLE I Lattice parameter, density and grain size of (Ti, V)C alloys

Compositon	Condition	a (nm)	$\varrho_{hp}/\varrho_{th}$ (%)	d (μm)
TiC	As-hot-pressed	0.432 614	~98.9	10
TiC–25% VC	As-hot-pressed	0.429 645	~99.7	24
TiC–50% VC	As-hot-pressed	0.425 116	~99.6	18
TiC–75% VC	As-hot-pressed	0.420 691	~99.5	17
TiC–75% VC	1900° C anneal	–	–	27
TiC–75% VC	2000° C anneal	–	–	48

Table I, ϱ_{hp} is the hot-pressed density and ϱ_{th} is the theoretical density. Pores were distributed both in the grains and along the grain boundaries. The average grain size, d, of TiC samples was 10 μm, while that of the other compositions was ~20 μm, as shown in Table I. The annealed samples showed no evidence of discontinuous grain growth. The average grain size of TiC–75% VC increased from the as-hot-pressed value of 17 to 48 μm after annealing at 2000° C for 1 h. The size and number of pores increased during static annealing. This degradation of microstructure occurs by evolution of CO/CO_2 gas [7]. The hot-pressed samples contain 0.6 to 0.9% unreacted carbon from the starting powders, as well as some from the graphite dies used in hot-pressing. The reaction of this carbon with the dissolved oxygen in the samples and oxygen in the argon forms CO/CO_2 which increases the porosity.

TEM examination indicated only a sparse distribution of dislocations. The matrix dislocations were primarily observed near the grain boundaries and along the second phase particles, resulting from the stress concentration at these sites. These observations also revealed the accumulation of impurities into second phase particles along the grain boundaries and in some of the triple junctions. Energy dispersive spectrometry data obtained with the STEM indicate that the particles contain cobalt, iron and nickel.

Diffraction patterns from as-hot-pressed TiC–VC alloys contain extra spots and streaks which result from ordering of vacancies on the carbon sublattice [2]. These features were absent in samples with no VC.

3.2. Stress–strain data

The true stress–true inelastic strain curves for TiC–50% VC alloys at temperatures between 1300 and 1600° C for both the loading and the relaxation portion of the deformation tests are shown in Figs 3a and b. Stress–strain curves for the other compositions are similar. On each sample, two to three load relaxation tests were performed at successively higher loads. The samples were deformed up to 15% plastic strain.

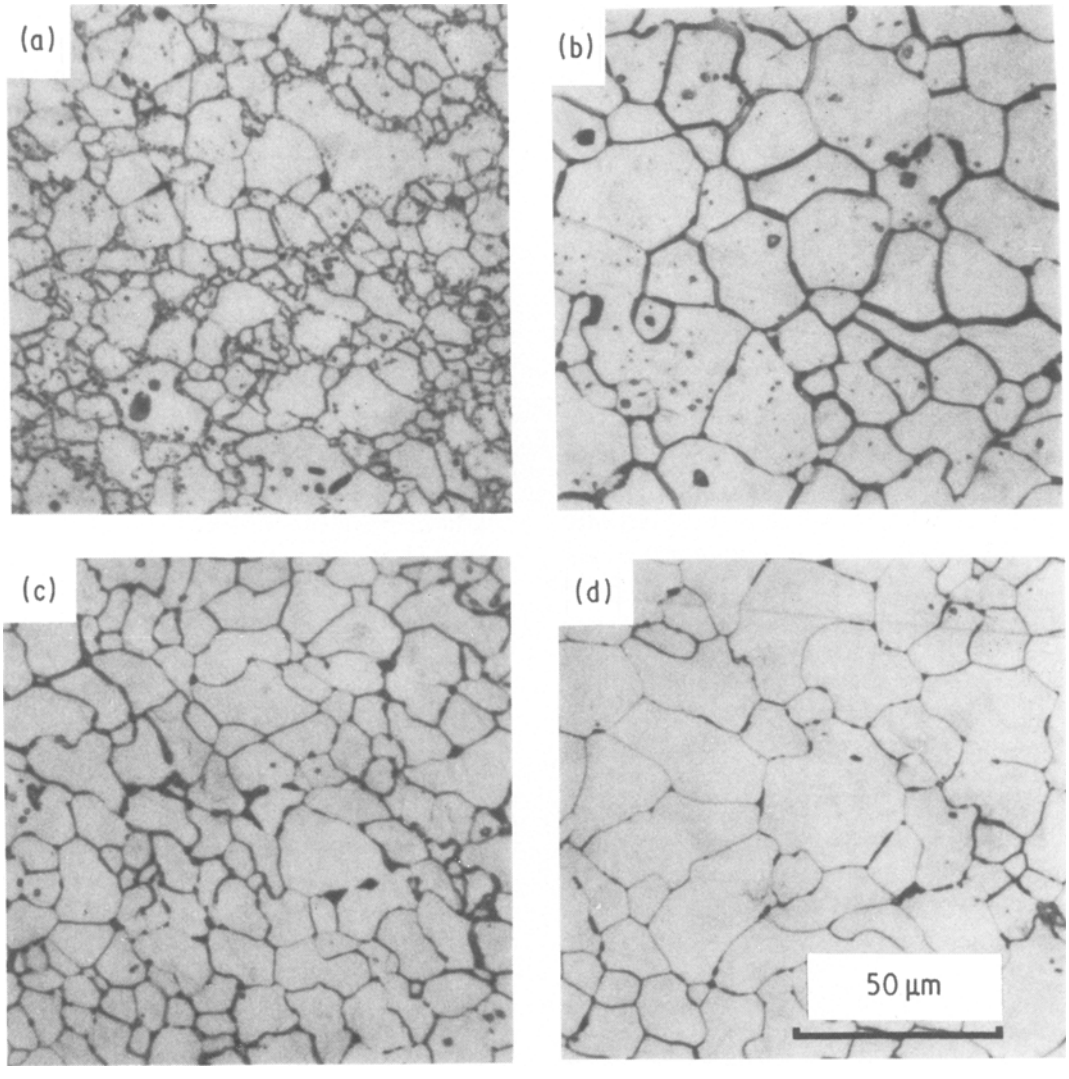

Figure 1 Optical micrographs of as-hot-pressed samples of (a) TiC, (b) TiC–25% VC, (c) TiC–50% VC, (d) TiC–75% VC.

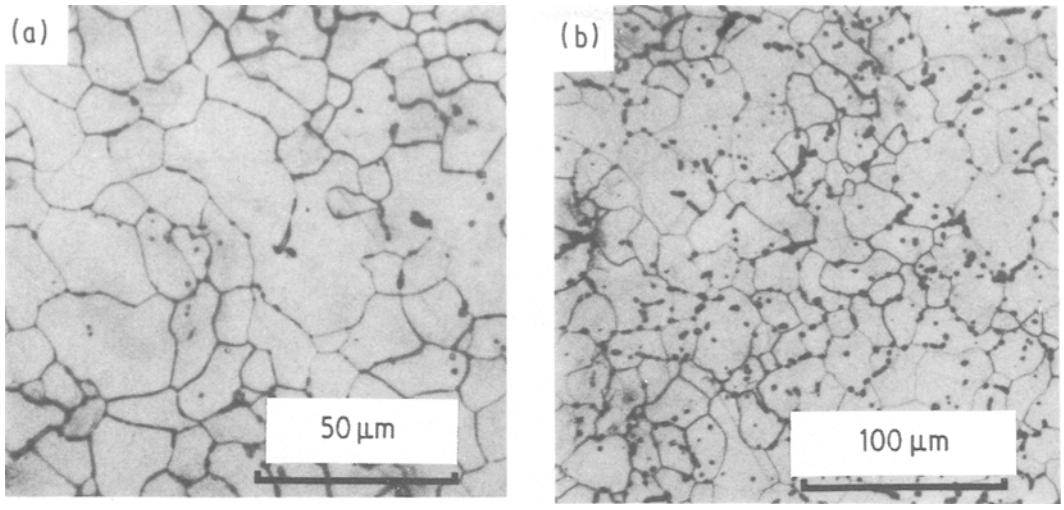

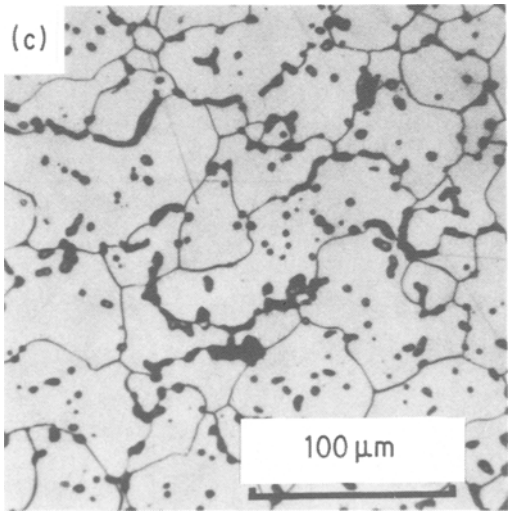

Figure 2 Optical micrographs of TiC–75% VC, (a) as-hot-pressed and annealed for 1 h at (b) 1900 and (c) 2000° C.

Note that the elastic component has been subtracted out of the raw data for these $\sigma-\varepsilon$ curves.

The following observations should be noted: (1) Samples could not be deformed plastically in the loading region except at higher temperatures (1500 to 1600° C), where samples yielded at ~75 to 100 MPa without a yield drop. (2) The amount of plastic strain incurred in the samples during the relaxation varied from 1 to 5%, depending on the load at which the relaxation was started.

3.3. Stress–strain rate data

The $\log\sigma-\log\dot{\varepsilon}$ curves for TiC–50% VC alloy, as shown in Fig. 4, were calculated from the load relaxation results obtained at temperatures between 1300 and 1600° C. The symbols and the relaxation numbers denote the successive relaxations at higher load. Generally each relaxation curve gave data over three orders of magnitude in strain rate. The following points can be made from this figure:

1. There is some transient behaviour during the initial period of relaxation, especially for relaxation data at 1300° C, in Fig. 4a. For a sample which could

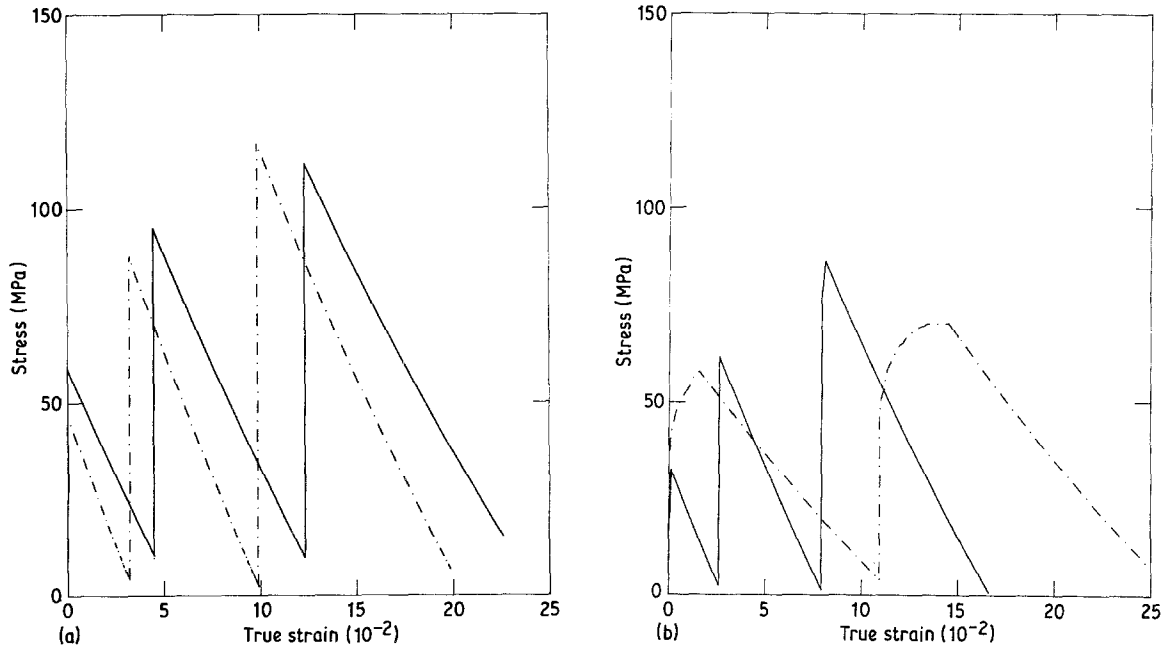

Figure 3 True stress–inelastic strain curves for TiC–50% VC for both the loading and the relaxation portions of the deformation tests. (a) (——) 1300° C, (–·—) 1400° C; (b) (——) 1500° C, (–·–) 1600° C.

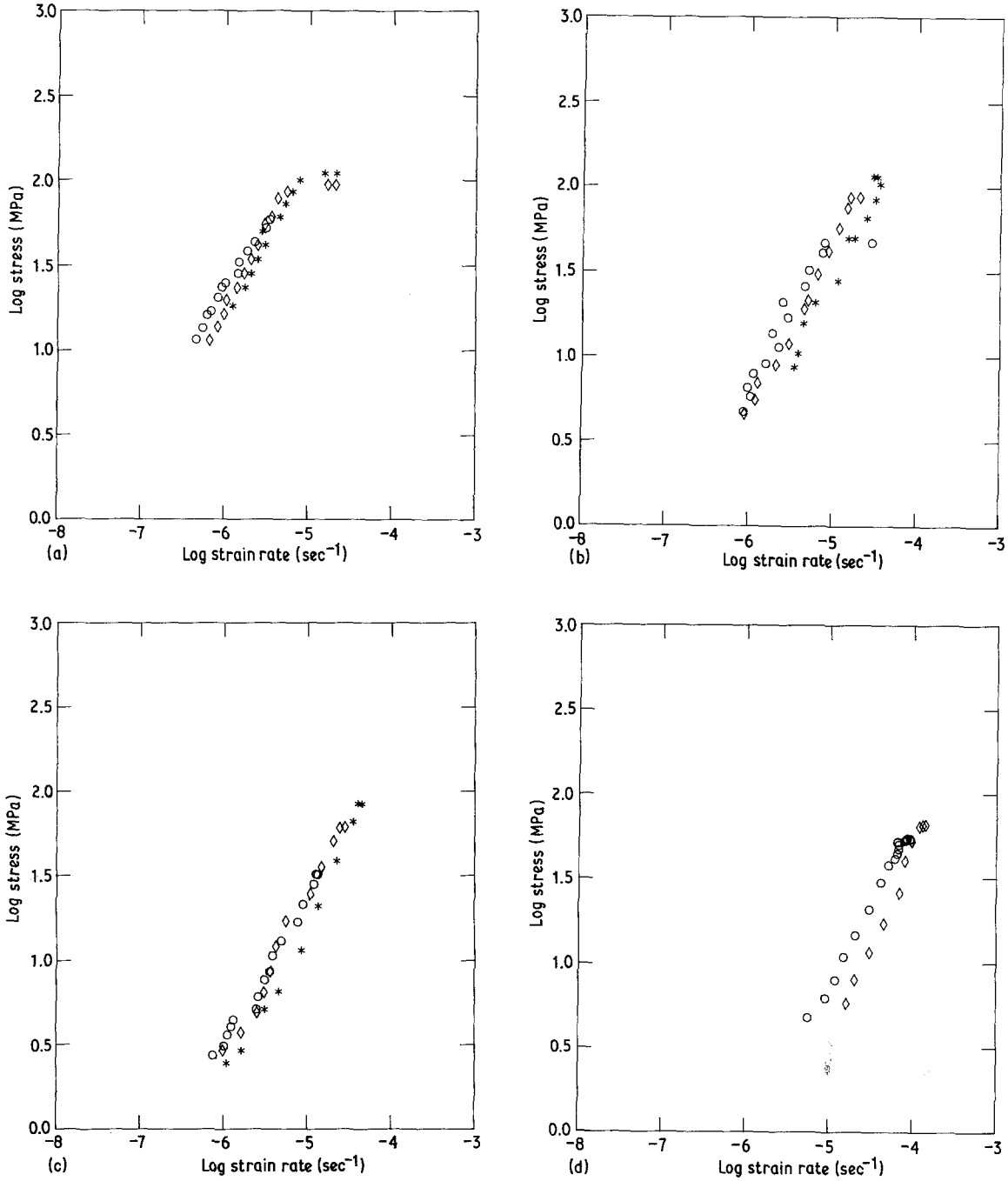

Figure 4 Log σ–log $\dot{\varepsilon}$ data for TiC–50% VC at different strain levels at (a) 1300, (b) 1400, (c) 1500, and (d) 1600° C. Relaxation = (○) 1, (◇) 2, (*) 3.

not be deformed plastically during loading, the strain rate for the stress level at the start of the relaxation was too high for significant plastic deformation to occur. Thus, primarily anelastic deformation occurred until the strain rate decreased to a value at which sample could deform primarily plastically [8]. The higher temperature data, Figs 4c and d, show less of this behaviour, as some plastic strain was accomplished in these samples during the loading region (Fig.3b); thus the samples deformed plastically from the start of the relaxation.

2. One striking feature of these log σ–log $\dot{\varepsilon}$ curves is that all of the curves for a given sample at a given temperature superimpose onto each other within the experimental error. This superposition suggests that the microscopic state variables remain essentially unchanged during the successive relaxations, and the deformation is steady state in nature.

3. The log σ–log $\dot{\varepsilon}$ curves for TiC–50% VC shift to the right in going from 1300 to 1600° C, (Fig. 4a to d) because of the decrease in the strength with increase in temperature.

4. The reciprocal of the slope of the log σ–log $\dot{\varepsilon}$ curves, that is, the strain rate sensitivity, $n = (\partial \log \dot{\varepsilon} / \partial \log \sigma)_T$ is ~ 1.0 for the TiC–50% VC alloy at all temperatures.

The load relaxation results for TiC, TiC–25% VC and TiC–75% VC show features similar to those discussed for TiC–50% VC. The strain rate sensitivity parameter varies between 1.4 and 0.9 for these compositions. Fig. 5 shows log σ–log $\dot{\varepsilon}$ response at 1300° C for TiC–75% VC as-hot-pressed, annealed at 1900° C, and annealed at 2000° C. These curves also exhibit features similar to those discussed for TiC. These results indicate that the strength of this alloy increases with increasing grain size.

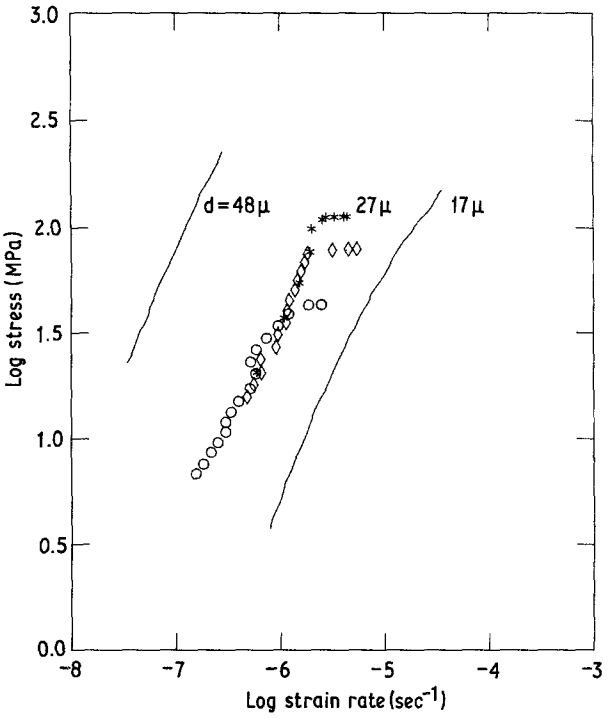

Figure 5 Log σ–log $\dot{\varepsilon}$ curves at 1300° C for TiC–75% VC samples which were simply hot-pressed, annealed at 1900° C for 1 h, and annealed at 2000° C for 1 h to yield grain sizes of 17, 25, and 48 μm, respectively. Relaxation = (○) 1, (◇) 2, (*) 3.

3.4. Deformation microstructure

The microstructures of the deformed samples are illustrated with TEM micrographs in Fig. 6. TEM examination revealed little evidence for dislocation activity in the deformed samples. These observations also indicated the presence of second phase particles along the grain boundaries. As mentioned earlier, these particles mainly consisted of cobalt, nickel and iron.

Some cracking was observed in the deformed samples. The cracks generally ran parallel to the axis of loading. It is believed that frictional forces (end effects) between the sample and the platens set up a triaxial state of stress. The stresses normal to the loading axis are tensile in nature, and the cracks form to relieve the stress during deformation.

4. Discussion

The absence of dislocations in the as-hot-pressed samples suggests that the densification may be controlled by diffusive mechanisms in (Ti, V)C. In hot-pressing experiments on these carbides [3], we found that the final stage densification is controlled by grain-boundary diffusion of carbon and/or metal. The effect of powder impurities on densification kinetics was also studied in detail. The impurities accumulate along the grain boundaries as second phase particles which have relatively low melting points. These low melting

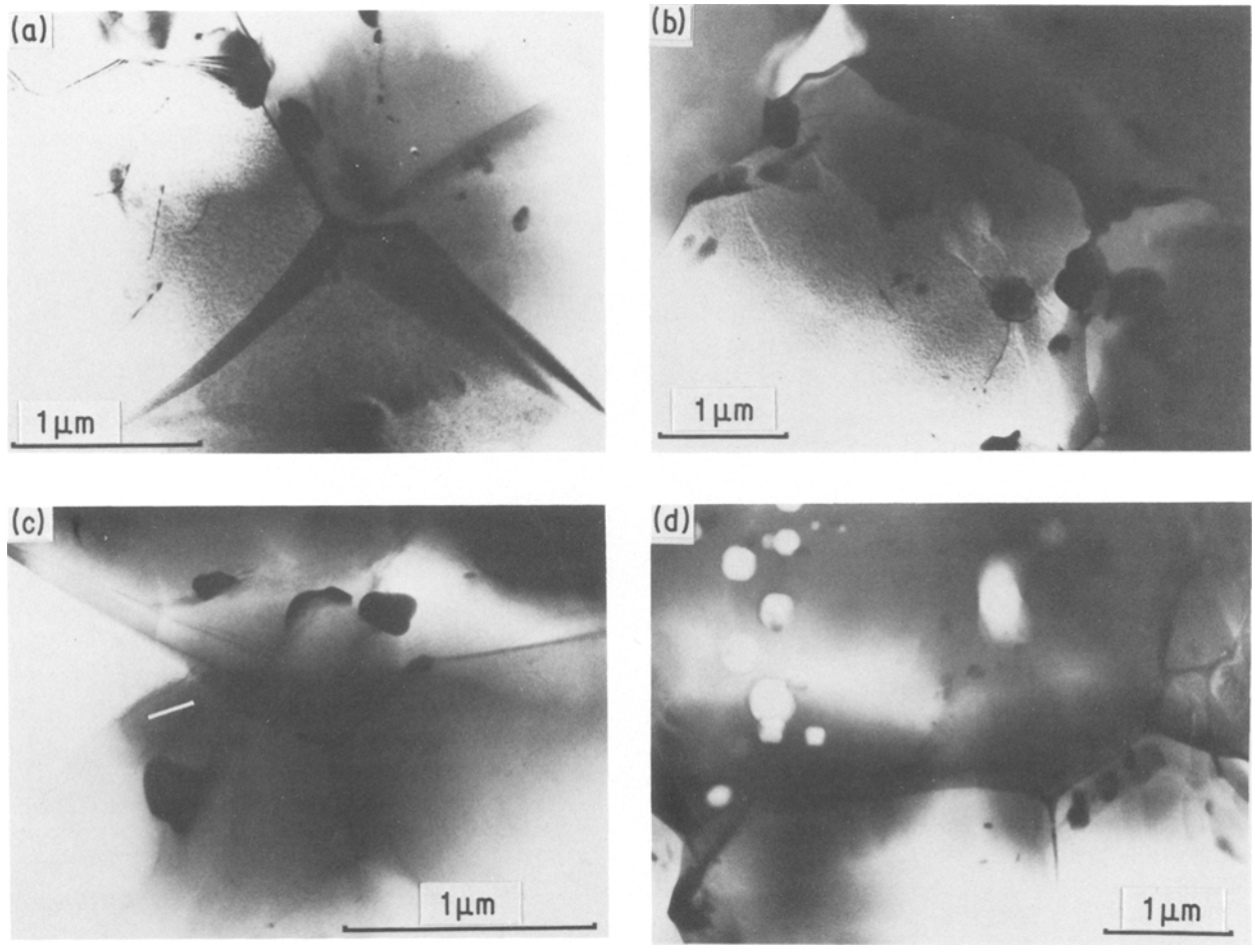

Figure 6 Bright-field TEM micrographs of TiC, deformed at 1500° C

point phases soften and/or melt between 600 and 1200° C, forming a liquid phase along at least portions of the grain boundaries, resulting in enhanced densification and grain growth in (Ti, V)C.

The extra spots and streaks in the diffraction patterns from the vanadium-bearing carbides are due to ordering of vacancies on the carbon sublattice. Vacancy ordering has been observed in VC throughout its composition range [9, 10] and in (Ti, V)C [2]. The order–disorder transition temperature is less than 1200° C for (Ti, V)C [11]. All the deformation experiments were carried out at or above this disordering temperature.

The stress–strain curves showed no yielding for TiC and (Ti, V)C alloys at 1200 and 1300° C up to the capacity of the testing machine, ~ 170 MPa. However, at higher temperatures, 1400 to 1600° C, the yield strength was found to be ~ 75 to 100 MPa. The yield strength of the polycrystalline TiC, ~ 400 MPa at 1200° C [12] and ~ 100 to 88 MPa at 1400 to 1600° C [13], is consistent with these results. Das *et al.* [14] observed somewhat higher values for the yield strength of polycrystalline TiC, ~ 600 to 400 MPa at 1200 to 1500° C. During the load relaxation experiments on single crystal TiC [15], we observed that the yield strength varies between ~ 135 MPa at 1200° C and 50 MPa at 1400°C.

The load relaxation curves for (Ti, V)C, Figs 4 and 5, exhibit steady state deformation behaviour with a strain rate sensitivity of $n \sim 1$. At 1300° C, the strength of TiC–75% VC increases with increasing grain size (Fig. 5). The microstructures on the deformed samples (Fig. 6) show little or no dislocation structure. These results suggest that the deformation is primarily controlled by diffusional flow, either by lattice diffusion (Nabarro–Herring creep [16, 17]) or grain-boundary diffusion (Coble creep [18]).

If the deformation is controlled by lattice diffusion, then the strain rate may be expressed as [16, 17]

$$\dot{\varepsilon} = 40 D_L \Omega \sigma / 3 d^2 k T \quad (7)$$

where D_L is the lattice diffusion coefficient, Ω an atomic volume, and k Boltzmann's constant. If the primary diffusion path is grain boundaries, then the strain rate is [18]

$$\dot{\varepsilon} = 47.5 D_b \Omega \delta \sigma / d^3 k T \quad (8)$$

where D_b is the grain-boundary diffusion coefficient and δ the grain-boundary width.

To determine which is the dominant mechanism of material transport during the deformation, the data from the load relaxation experiments on TiC–75% VC at 1300° C (Fig. 5) are plotted as $\ln \sigma - \ln \dot{\varepsilon}$ against $\ln d$ in Fig. 7. From this curve, the grain size exponent was found to be ~ 2.6, suggesting that the plastic deformation of (Ti, V)C is controlled by grain-boundary diffusion. This result is in agreement with our hot-pressing results [3], where it was found that the grain-boundary diffusion is the predominant mechanism of densification.

Thus, the load relaxation data were analysed in terms of Equation 8 and the diffusion coefficients for (Ti, V)C at various temperatures were determined.

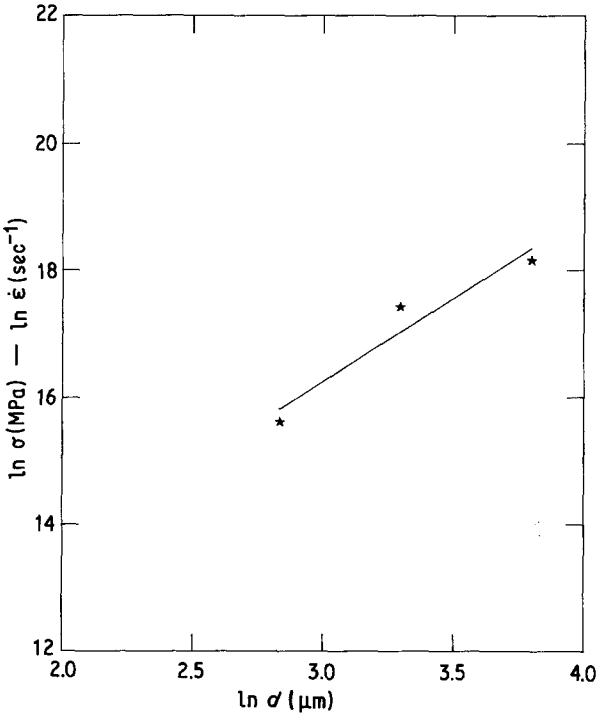

Figure 7 Calculation of the grain size exponent from the plot of $\ln \sigma - \ln \dot{\varepsilon}$ against $\ln d$ for TiC–75% VC at 1300° C, $m = 2.6$.

The atomic volumes were calculated from the measured lattice parameters, Table I, and a value of 1 nm was used for grain boundary width [19].

The calculated values for the boundary diffusivities for four compositions of (Ti, V)C are shown on an Arrhenius plot in Fig. 8. The results of the present study are compared with those reported in literature for carbon and metal diffusion in either TiC or VC. No data are available on diffusion in (Ti, V)C. Sarian [20–22] determined the diffusion coefficients for carbon and titanium self-diffusion in TiC_x, as well as

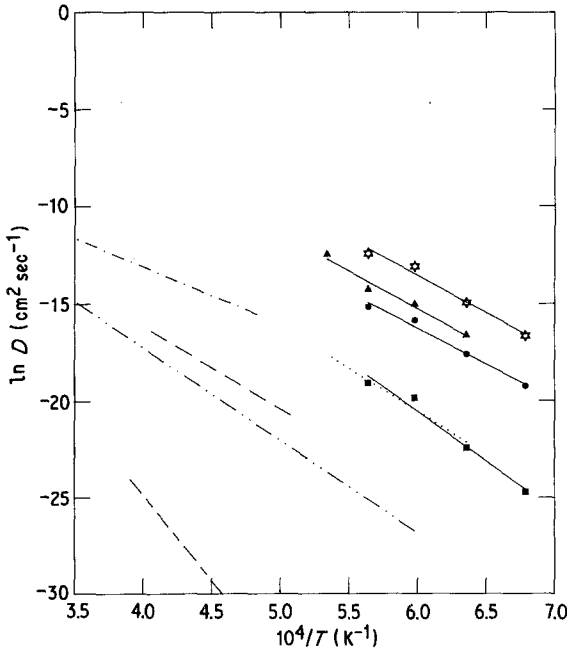

Figure 8 Arrhenius plot of diffusion coefficients of carbon and metal in (Ti, V)C. (–·–) Adelsberg and Cadoff [23], (···) Quinn and Kohlstedt [24], (–··–) Sarian (C in TiC) [20], (– – –) Sarian (Ti in TiC) [21], (— —) Sarian (C in $VC_{0.84}$) [22], (——) present study. (■) TiC, (●) TiC–25% VC, (▲) TiC–50% VC, (✡) TiC–75% VC.

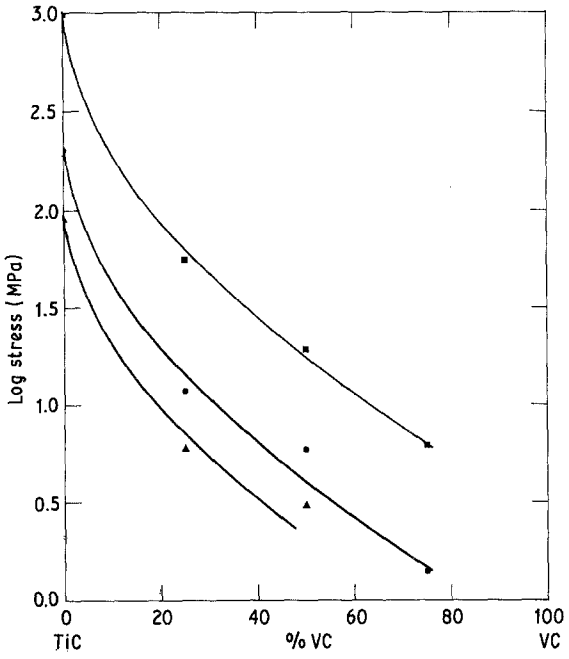

Figure 9 Variation of strength of (Ti, V)C with %VC at (■) 1300, (●) 1400, (▲) 1500° C. The stress was determined from the load relaxation data at $\dot{\varepsilon} \sim 1 \times 10^{-6}\,\text{sec}^{-1}$ and normalized to a fixed grain size of 20 μm.

for carbon self-diffusion in $VC_{0.84}$ single crystals by tracer techniques. These values represent lattice diffusion of carbon and metal in the carbides. The data of Adelsberg and Cadoff [23] represent short circuit diffusion of carbon along grain boundaries, as these diffusivities were determined by carburization of metal. The work by Quinn and Kohlstedt [24] on the TiC–Ti diffusion couple yielded similar results.

The diffusion coefficients obtained in this study lie considerably above the tracer (lattice) diffusion coefficients and are in good agreement with those obtained for boundary diffusion, supporting the previous conclusion that the plastic deformation is controlled by diffusive flux of metal and/or carbon atoms along the grain boundaries. The activation energy for diffusion, evaluated from Fig. 8, is $\sim 390\,\text{kJ mol}^{-1}$ for TiC and $\sim 307 \pm 13\,\text{kJ mol}^{-1}$ for other compositions.

It can be seen in Fig. 8, that, at a given temperature, the diffusion coefficients determined for (Ti, V)C increases with the addition of VC, resulting in a faster rate of deformation. The same conclusion can be drawn from the $\log\sigma$–$\log\dot{\varepsilon}$ curves which shift to the right in going from TiC to TiC–75% VC, demonstrating a decrease in strength with the addition of VC. This behaviour is amplified in Fig. 9 in which $\log\sigma$ at $\dot{\varepsilon} \sim 10^{-6}\,\text{sec}^{-1}$, determined from the load relaxation results and normalized to a fixed grain size of 20 μm using Equation 8, is plotted against composition for three temperatures. It is clear that the strength of (Ti, V)C decreases with the addition of VC.

This result differs from the findings by Hollox *et al.* [1] on single crystals of (Ti, V)C which, as stated earlier, indicate a maximum in critical resolved shear stress at TiC–67% VC. They have explained their observations in terms of the Peierls stress, a dispersed ordered phase in a disordered matrix and an electronic structure giving rise to an anomalously low lattice parameter for TiC–60% VC. Their analysis cannot be applied to the present study, as the deformation is mainly controlled by grain-boundary diffusion instead of dislocation creep. The room temperature hardness of (Ti, V)C is influenced by the ordering of vacancies and in turn by the cooling rate, therefore no comparison can be made of these results [1, 2] with the high temperature deformation properties.

To explain the decrease in the strength of (Ti, V)C with the addition of VC, the effect of various parameters on the strength of (Ti, V)C has to be examined. The shear moduli for TiC and VC are $\sim 2 \times 10^5$ and 1×10^5 MPa, respectively; while the melting points of $TiC_{0.97}$ and $VC_{0.88}$ are 2776 and 2625° C, respectively [6, 25]. TiC and VC form a continuous solid solution [6], thus it might be expected that the strength of (Ti, V)C single phase alloys should decrease slightly with the addition of VC. However, the drastic reduction in the strength of (Ti, V)C with the addition of VC, Fig. 9, cannot be explained just in terms of shear modulus and melting temperature.

The effect of second phase material rich in cobalt, iron, nickel and chromium along the grain boundaries on the mechanical properties of TiC has been studied in detail previously [7, 12, 14]. These studies have revealed that a sharp drop in the bending strength at ~ 1000 to 1200° C, which is accompanied by a transition from primarily transgranular fracture at lower temperatures to predominantly intergranular fracture at higher temperatures, is due to a softening and/or melting of an impurity film at the grain boundaries.

Similarly, in our experiments the decrease in the strength of the (Ti, V)C alloys with the addition of VC can be attributed to the powder impurities. VC powder has a higher concentration of impurities and free carbon than does the TiC powder (Table II of companion paper [3]). As discussed in our hot-pressing experiments on (Ti, V)C [3], these impurities form low-melting point phases by complex eutectic reactions with each other and with the free carbon. As both titanium and vanadium form a series of oxides [26, 27], oxygen in the starting powders can also have considerable influence on high temperature mechanical properties; for example, in the V_2O_3–V_2O_5 system a liquid phase forms due to a eutectic reaction at ~ 600° C. A localized liquid phase will be redistributed along the grain boundaries during hot-pressing. Because the grain boundaries in VC are more readily wet than those in TiC [28, 29], the liquid phase may more drastically reduce the strength of the VC-rich samples.

Various attempts have been made to study the deformation behaviour of polycrystalline transition metal carbides. Martin *et al.* [30] performed four point bending experiments on thin sheets of TaC_x with average grain size ~ 0.1 mm. They described the plastic deformation in terms of carbon diffusion assisted movement of dislocations. Similar behaviour is reported by Darolia and Archbold [31] from the measurement of compressive yield strength of ZrC with average grain size of 0.25 mm. The mechanical

properties of fine-grained TiC, ~7 to 8 μm, were studied by Das *et al.* [14] and Chermant *et al.* [13], using both bending and compression tests. According to these authors, at moderate temperatures (< 1500 to 1600° C) dislocation movement is controlled by the diffusion of carbon; while at higher temperatures deformation is controlled by the diffusion of titanium. All these observations were based on the deformation at the yield point with the strain rates between 10^{-1} and 10^{-4} sec^{-1}. In the present study, large plastic deformation at much slower strain rates, 10^{-4} to 10^{-7} sec^{-1}, was studied. Thus, the deformation by diffusional flow in fine-grained (Ti, V)C alloys at slower strain rates and smaller stresses is consistent with the reported results.

Acknowledgements

This research was supported by the Department of Energy through grant number DE-AC02-77ER04441. The electron microscopy was carried out in the Central Facility for Electron Microscopy which is part of the Materials Science Center at Cornell University.

References

1. G. E. HOLLOX, D. L. NOVAK and R. D. HUNTINGTON, Proceedings of the Second International Conference on the Strength of Metals and Alloys (ASM, Metals Park, Ohio, 1970) p. 1192.
2. R. H. J. HANNINK and M. J. MURRAY, *Scr. Met.* **9** (1975) 1271.
3. V. M. SURA and D. L. KOHLSTEDT, *J. Mater. Sci.* **21** (1986) 2347.
4. I. LERNER, S.-W. CHIANG and D. L. KOHLSTEDT, *Acta Met.* **27** (1979) 1187.
5. E. W. HART and H. D. SOLOMON, *ibid.* **21** (1973) 295.
6. E. RUDY, "Compendium of Phase Diagram Data" AFML-TR-65-2, Part V (Air Force Materials Laboratory, Wright-Paterson AFB, Ohio, 1969) p. 251–2.
7. A. P. KATZ, H. A. LIPSITT, T. MAH and M. G. MENDIRATTA, *J. Mater. Sci.* **18** (1983) 1983.
8. E. W. HART, C.-Y. LI, H. YAMADA and G. L. WIRE, in "Constitutive Equations in Plasticity", edited by A. S. Argon (MIT Press, Cambridge, Massachusetts, 1975) p. 149.
9. C. FROIDEVAUX and D. ROSSIER, *J. Phys. Chem. Solids* **28** (1967) 1197.
10. J. D. VENEABLES, D. KAHN and R. G. LYE, *Phil. Mag.* **18** (1968) 177.
11. R. H. J. HANNINK and M. J. MURRAY, International Crystallography Conference on Diffraction Studies of Real Atoms and Real Crystals, Melbourne (Australian Academy of Science, Canberra, 1974) p. 239.
12. D. B. MIRACLE and H. A. LIPSITT, *J. Amer. Ceram. Soc.* **66** (1983) 592.
13. J. L. CHERMANT, G. LECLERC and B. L. MORDIKE, *Z. Metallkde.* **71** (1980) 465.
14. G. DAS, K. S. MAZDIYASNI and H. A. LIPSITT, *J. Amer. Ceram. Soc.* **65** (1982) 106.
15. V. M. SURA and D. L. KOHLSTEDT, *ibid.* in press.
16. F. R. N. NABARRO, Bristol Conference on Strength of Solids, Bristol, England, April 1948 (The Physical Society, London, 1948) p. 75.
17. C. HERRING, *J. Appl. Phys.* **21** (1950) 437.
18. R. L. COBLE, *ibid.* **34** (1963) 1679.
19. N. L. PETERSON, *Int. Met. Rev.* **28** (1983) 65.
20. S. SARIAN, *J. Appl. Phys.* **40** (1969) 3515.
21. *Idem, ibid.* **39** (1968) 3305.
22. *Idem, J. Phys. Chem. Solids* **33** (1972) 1637.
23. L. M. ADELSBERG and L. H. CADOFF, *Trans. AIME* **239** (1967) 933.
24. C. J. QUINN and D. L. KOHLSTEDT, *J. Amer. Ceram. Soc.* **67** (1984) 305.
25. L. E. TOTH, "Transition Metal Carbides and Nitrides" (Academic, New York, 1971) p. 75.
26. E. M. LEVIN, C. R. ROBBINS and H. F. MuMURDIE, "Phase Diagram for Ceramists", (American Ceramic Society, Columbus, Ohio, 1975) p. 41.
27. E. M. LEVIN and H. F. MuMURDIE, "Phase Diagrams for Ceramists, 1975 Supplement", (American Ceramic Society, Columbus, Ohio, 1975) p. 16.
28. R. WARREN and M. B. WALDRON, *Powder Metall.* **15** (1972) 166.
29. R. WARREN, *J. Mater. Sci.* **15** (1980) 2489.
30. J. L. MARTIN, P. LACOUR-GAYET and R. COSTA, in Proceedings of Fifth International Materials Symposium, Berkeley, California, March 1972, edited by Gareth Thomas (University of California, 1972) p. 1131.
31. R. DAROLIA and T. F. ARCHBOLD, *J. Mater. Sci.* **11** (1976) 283.

Received 16 July
and accepted 13 September 1985